

A solid-state NMR three-qubit homonuclear system for quantum information processing: control and characterization

Jonathan Baugh,* Osama Moussa, Colm A. Ryan, and Raymond Laflamme†
*Institute for Quantum Computing,
 University of Waterloo, Waterloo, Ontario N2L 3G1*

Chandrasekhar Ramanathan, Timothy F. Havel, and David G. Cory
*Department of Nuclear Science and Engineering,
 Massachusetts Institute of Technology,
 Cambridge, MA 02139*

(Dated: December 26, 2018)

A three-qubit ^{13}C solid-state nuclear magnetic resonance (NMR) system for quantum information processing, based on the malonic acid molecule, is used to demonstrate high-fidelity universal quantum control via strongly-modulating radio-frequency pulses. This control is achieved in the strong-coupling regime, in which the timescales of selective qubit addressing and of two-qubit interactions are comparable. State evolutions under the internal Hamiltonian in this regime are significantly more complex, in general, than those of typical liquid-state NMR systems. Moreover, the transformations generated by the strongly-modulating pulses are shown to be robust against the types of ensemble inhomogeneity that dominate in the employed molecular crystal system. The secondary focus of the paper is upon detailed characterization of the malonic acid system. The internal Hamiltonian of the qubits is determined through spectral simulation. A pseudopure state preparation protocol is extended to make a precise measurement of the dephasing rate of a three-quantum coherence state under residual dipolar interactions. The spectrum of intermolecular ^{13}C - ^{13}C dipolar fields in the crystal is simulated, and the results compared with single-quantum dephasing data obtained using appropriate refocusing sequences. We conclude that solid-state NMR systems tailored for quantum computing have excellent potential for extending the investigations begun in liquid-state systems to greater numbers of qubits in a more general setting.

PACS numbers: 03.67.Lx, 61.18.Fs, 76.60.-k

I. INTRODUCTION

Quantum computing (QC) aims to achieve the ultimate in computational power from physical systems by exploiting their quantum nature [1]. Nuclear magnetic resonance (NMR)-based QC has been successfully implemented in liquid-state ensemble systems of up to 7 qubits [2, 3, 4, 5, 6, 7], and more recently in a 12 qubit system [8]. Universal quantum control is achieved through application of external radio-frequency (RF) fields on or near resonance with spin transitions of a set of separately addressable, coupled spins. State initialization (to a fiducial state such as $|00..0\rangle$) is effectively achieved in these systems by the preparation of pseudopure states [2, 9]. A hallmark of control in these systems is a separation of timescales between (faster) qubit addressability and (slower) two-qubit coupling gates, typically by an order of magnitude or more [5]. For the homonuclear subsystems, this corresponds to the weak-coupling regime, in which the relative Zeeman shifts in the qubit

Hamiltonian are significantly larger than the J -couplings [10, 11]. This results in a suppression of the transverse spin-operator coupling terms that do not commute with the Zeeman shift operators, leading to an effectively diagonal spin Hamiltonian, and therefore to coupling evolutions that are purely controlled-phase evolutions. In this work, we examine NMR-based QC implemented in a *solid-state* homonuclear system, in which the qubit Hamiltonian is no longer in the weak-coupling regime. A solid-state NMR architecture is attractive due to several key properties [5]: (1) nuclear spin states can be purified by practical means to near-unity polarizations [12]; (2) intrinsic decoherence times can be much longer, and two-qubit gate times much shorter, than those in the liquid state; (3) the qubit spins can be brought into well-controlled contact with a thermal-bath of bulk spins, enabling entropy-reducing operations such as algorithmic cooling [13, 14] and quantum error correction [15, 16] to be carried out. The system we will describe is specially tailored so that the ensemble description of the system is—to a good approximation—analogous to that of liquid-state NMR-QC, and therefore the general aspects of control and measurement are the same [5, 17]. However, we will demonstrate that universal, coherent control can be implemented in this strong-coupling regime: the regime in which the timescales of qubit addressing and qubit

*Electronic address: baugh@iqc.ca

†Electronic address: rlaflamme@iqc.ca; URL: <http://www.iqc.ca>; Also at Perimeter Institute for Theoretical Physics, Waterloo, ON

coupling are comparable. In this regime, the transverse spin operator terms from qubit-qubit dipolar couplings are not fully suppressed by the relative Zeeman shift operators. These residual 'flip-flop' terms $\sigma_+^j \sigma_-^k + \sigma_-^j \sigma_+^k$ (where $\sigma_{\pm} = \sigma_x \pm i\sigma_y$ and $\{\sigma_x, \sigma_y\}$ are Pauli matrices) render the state evolutions more complex, in general, than those of typical liquid-state NMR systems. We show that strongly-modulating pulses [18] succeed in controlling the solid-state QC system, with generality and with high-fidelity. Moreover, the pulses provide significant robustness for the desired transformations against the ensemble inhomogeneities that are typical of solid-state NMR systems. This latter property is of great importance to the practical application of quantum algorithms in such systems, and we present here a first step in its study. This control methodology is a key ingredient in the realization of solid-state NMR-QC testbed devices, but could also extend to many other potential systems for quantum information processing. We also remark that liquid-crystalline NMR-QC implementations [7, 19] represent a coupling regime that is typically intermediate between the strong- and weak-coupling cases. Strongly-modulating pulses would therefore be an appropriate means for controlling such systems universally.

The secondary focus of this paper is to characterize, in detail, the employed three-qubit system based on the malonic acid molecule. This includes characterization of the dominant ensemble inhomogeneities arising both through linear and bi-linear terms in the Hamiltonian. In tailoring the present system, we have used dilution of the qubit molecules as a means for reaching an approximate ensemble description in which processor molecules are, ideally, non-interacting and reside in identical environments. However, the need for a macroscopic number of spins to generate observable NMR signals through the usual inductive detection both limits the degree of dilution and requires a macroscopic sample. The former results in perturbing intermolecular dipolar fields, and the latter typically yields significant inhomogeneities of applied magnetic fields over the sample volume, namely, the static magnetic field and the RF amplitude. Inhomogeneity of the static magnetic field leads to a dispersion of Zeeman shifts; similar Zeeman dispersion may also arise from the effect of crystal strain on the anisotropy of chemical shielding [25]. In this paper, we address the robustness of strongly-modulating pulse control to dispersion of Zeeman shifts and of RF amplitudes. We also characterize in detail the intermolecular dipolar environment in the present system, but leave the study of its effects on quantum gate implementation for future work.

The paper is organized as follows: section II reviews strongly-modulating RF pulses as a means of achieving universal quantum control, and numerical results for an example pulse are discussed; in section III, the dilute ^{13}C malonic acid system is first characterized; section IV demonstrates the preparation of a pseudopure state (as a benchmark for control) and analyzes the results; section IV C treats an application of the

pseudopure state protocol: precise measurement of the triple-quantum dipolar dephasing rate, and comparison to single-quantum dephasing rates; in section V, simulated and experimental data are presented that explore the effect of intermolecular dipolar couplings on qubit coherence times; in section V B, a multiple-pulse refocusing sequence is used in order to compare appropriate experimental quantities with the intermolecular dipolar simulations, and as a first step in testing the attainability of long ensemble coherence times in this system; the overall results are discussed in section VI, in the context of assessing the future goals and potential of solid-state NMR-QC.

II. UNIVERSAL CONTROL: STRONGLY-MODULATING PULSES

Numerically optimized 'strongly-modulating' pulses were introduced by the MIT Cory group as a means of implementing fast, high-fidelity unitary gate operations in the context of liquid-state NMR-QC [18]. The aim is to construct an arbitrary modulated RF waveform that, when applied to the system, generates a desired effective Hamiltonian corresponding to a particular quantum gate. This is accomplished numerically by minimizing the distance between the actual and the desired unitary transformations using a simplex search algorithm. Gate fidelities are defined by the expression:

$$F = \sum_{\mu} p_{\mu} |Tr(U_{des}^{\dagger} U_{calc}^{\mu})/N|^2 \quad (1)$$

where N is the dimension of the Hilbert space, U_{des} is the desired unitary and U_{calc} is the unitary calculated for the evolution of the system under the modulated RF pulse. p_{μ} is a normalized empirical distribution over an inhomogeneous parameter (or parameters) of the ensemble, typically the RF amplitude. The expression for F corresponds to an average fidelity over all possible input states [18]. The number of parameters the algorithm must search over is made minimal by requiring the modulating waveform to consist of a series of constant amplitude and frequency periods, so that each period has a time-independent Hamiltonian in a particular rotating reference frame [18]. Modulation pulses with ideal (simulated) fidelities of order $F \sim 99\%$ are readily found for liquid-state NMR-QC systems with up to 6 qubits [8, 18].

It is observed empirically that good modulating pulse solutions tend to have the average RF amplitude $\nu_{RF} \sim |\mathcal{H}|$, where $|\mathcal{H}|$ is the magnitude of the internal qubit Hamiltonian. It is precisely this strong driving regime in which analytical techniques (e.g. perturbation theory) for calculating dynamics break down, yet the system generally has the broadest (and most rapid) access to the manifold of allowed states. It is also the regime in which all accessible spin transitions are excited, so that refocusing of unwanted interactions becomes possible, even

to the extent that the dephasing effects of ensemble inhomogeneities may be partially suppressed.

An example of a strongly modulating RF pulse is shown in Fig. 1. The pulse is tailored to generate a three-qubit controlled-(not \otimes not) gate in the strongly-coupled malonic acid system to be described in the next section. The average RF amplitude is 9.4 kHz, whereas the magnitude of the internal ^{13}C Hamiltonian (parameters listed in Table I, next section) is 7.3 kHz. Part (c) of the figure demonstrates the robustness of the calculated unitary over the dominant inhomogeneous Hamiltonian parameters of the ensemble, namely, scaling of the RF amplitude and dc field offset. This pulse was optimized over a probability distribution p_μ of RF amplitude scaling, centered on unity, with standard deviation $\sigma(p_\mu) \simeq 6\%$. The fact that the unitary fidelity is $> 90\%$ over a 1 kHz range of dc field offset demonstrates the ability of the modulated pulse to effectively refocus evolution under Zeeman shift dispersion (no Zeeman distribution was used in the optimization). The ideal fidelity $\sim 98\%$ obtained here is impressive considering the challenge of finding control sequences in the strong-coupling regime; however, even greater precision is likely required for successful implementation of quantum algorithms in general. We consider this a first step, and one that can be significantly improved upon in future work.

The strongly-modulating pulse optimization is also ideal for finding nearly time-optimal pulses. For example, the gate shown in Fig. 1 involves simultaneous control-not operations using C_m as the control qubit. Since both dipolar couplings to C_m are $d_{jm} \sim 1$ kHz (see next section-Table I), this suggests a lower bound on the possible gate time of at least $\sim \frac{1}{4D} \simeq 250\mu\text{s}$. However, the real lower bound is probably somewhat longer due to the fact that some selective qubit excitation is necessary in addition to the coupling evolution, and the timescale for the selective addressing is set by the relative Zeeman shifts of the qubits. Although the example pulse of Fig. 1 has a duration $\simeq 700\mu\text{s}$, we have found pulse solutions for the same gate (fidelities $> 90\%$) as short as $\simeq 450\mu\text{s}$, which is probably close to the time-optimal solution.

III. CHARACTERIZATION I: ENSEMBLE HAMILTONIAN

A. Single-crystal malonic acid, dilute ^{13}C -labelling

The system under study is single crystal malonic acid grown from aqueous solution with a dilute fraction of fully ^{13}C labelled molecules. The main crystal used herein has dimensions of $4 \times 1.5 \times 1.5$ mm 3 and a labelled molecule fraction of 3.2% (a similar crystal with 1.6% dilution was used in the experiments of section V B). For the malonic acid molecule in the solid, the three carbon nuclei have distinct anisotropic chemical shielding tensors so that when placed in a large static magnetic field, crystal orientations can be found for which each carbon

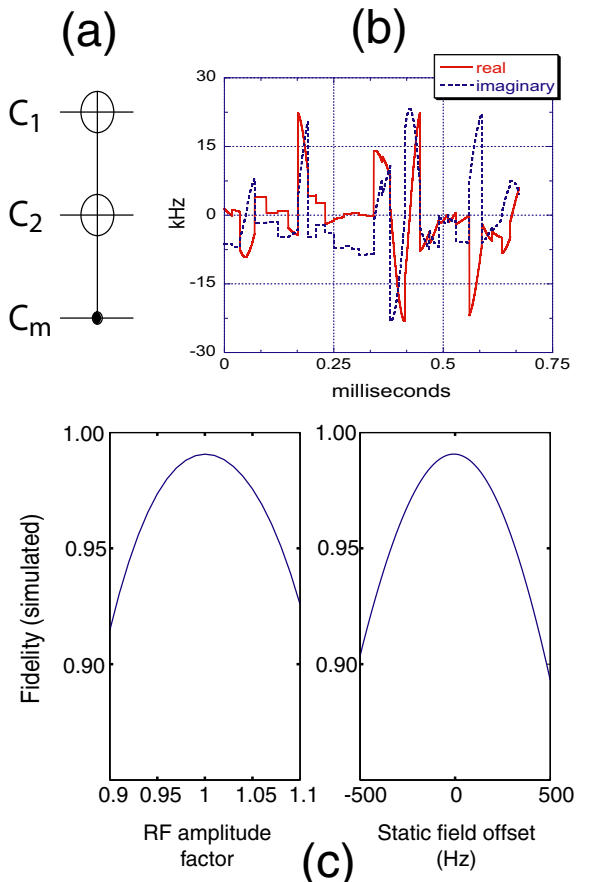


FIG. 1: Example of a modulated RF pulse solution for generating a three-qubit gate in the malonic acid system. (a) quantum network representation of the gate, which is a controlled-(not \otimes not), with C_m as the control bit and C_1 and C_2 as target bits. (b) the quadrature components of the RF modulation waveform, labelled 'real' and 'imaginary'. (c) Simulated fidelity of the transformation as a function of (left) scaling of the RF amplitude and (right) offset of the dc magnetic field.

is separately addressable in frequency. Protons, of which there are four per molecule (and are 100% abundant in the crystal), can be used to cross-polarize the carbon spins, and are otherwise decoupled from the ^{13}C system. Figure 2 shows the malonic acid unit cell as determined by x-ray diffraction [20]. The space group is P-1 so that the two molecules in the unit cell are related by inversion symmetry, and are therefore magnetically equivalent. The crystal orientation is chosen to maximize the intramolecular ^{13}C - ^{13}C dipolar couplings and the relative ^{13}C Zeeman shifts. The full spin Hamiltonian of the system is:

$$\mathcal{H}(t) = \mathcal{H}_C + \mathcal{H}_H + \mathcal{H}_{CH} + \mathcal{H}_{RF}(t) \quad (2)$$

where \mathcal{H}_C and \mathcal{H}_H are the ^{13}C and ^1H Hamiltonians, \mathcal{H}_{CH} is the interspecies coupling Hamiltonian, and $\mathcal{H}_{RF}(t)$ is the time-dependent Hamiltonian of the external radio-frequency field. In many experiments, $\mathcal{H}_{RF}(t)$

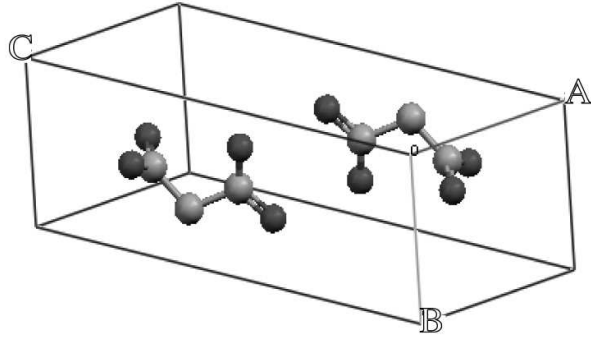


FIG. 2: Unit cell of malonic acid, with crystal axes indicated. The two molecules are related by inversion symmetry, and are therefore magnetically equivalent (P-1 space group). The light (dark) atoms are carbon (oxygen), and the hydrogen atoms are not shown. $\vec{A} = 5.156\text{\AA}$, $\vec{B} = 5.341\text{\AA}$ and $\vec{C} = 8.407\text{\AA}$ [20].

includes a strong field resonant with the ^1H spins so that \mathcal{H}_{CH} is effectively removed from the Hamiltonian. The ^{13}C Hamiltonian can be decomposed as:

$$\mathcal{H}_C = \mathcal{H}_{CZ} + \mathcal{H}_{CD}^{intra} + \mathcal{H}_{CD}^{inter} \quad (3)$$

where the terms on the right side, from left to right, are the Zeeman, the intramolecular dipolar, and the intermolecular dipolar terms. The Zeeman and intramolecular dipolar terms dominate the natural ^{13}C Hamiltonian in the dilute ^{13}C crystal, and will be used (along with the RF) in the construction of quantum gates. The intermolecular couplings act as perturbations on these terms, and their effects will be examined in section V. Denoting single-spin Pauli matrices as $X = \sigma_x$, $Y = \sigma_y$, $Z = \sigma_z$, the Zeeman and intramolecular dipolar terms may be expressed as:

$$\mathcal{H}_{CZ} = \sum_{j=1}^3 \frac{\nu_j}{2} Z^j \quad (4)$$

$$\mathcal{H}_{CD}^{intra} = \sum_{m < n} \frac{d_{mn}}{4} (2Z^m Z^n - Y^m Y^n - X^m X^n) \quad (5)$$

where $\{m, n = 1, 2, 3\}$, ν_j are the rotating-frame Zeeman frequencies and d_{mn} are the dipolar coupling strengths. Table I lists these parameters, as obtained from fitting the ^{13}C spectrum of Figure 3, for the crystal orientation used throughout. It also lists the free-induction dephasing times, T_2^* ; the corresponding rates $(T_2^*)^{-1}$ provide a measure of the degree of ensemble inhomogeneity. It will be seen in section V. that the dominant contribution to these rates is Zeeman shift dispersion, most likely due to inhomogeneity of the static NMR field through the crystal.

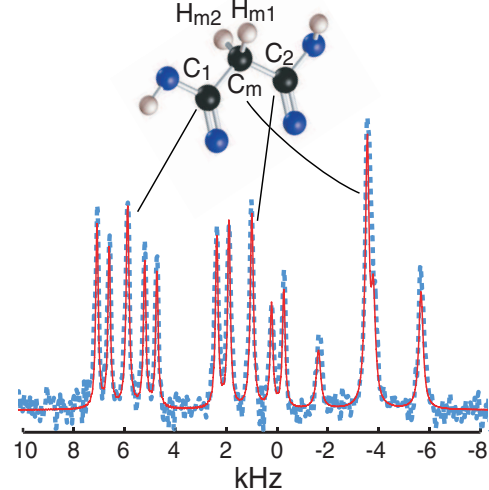


FIG. 3: ^{13}C -NMR spectrum (dotted line) and spectral fitting results (solid line) for 3.2% ^{13}C -labelled malonic acid in the crystal orientation used throughout. The fitting procedure adjusts the simulated Hamiltonian to match the spectrum, and uses Lorentzian line broadening to fit the $(T_2^*)^{-1}$ dephasing rates. Proton decoupling was applied using a TPPM sequence [21] at an RF power of 250 kHz. Note the most intense peaks, in the center of each multiplet, correspond to the natural abundance (1.1%) ^{13}C . The uneven heights of the labelled-molecule peaks indicate that the relative Zeeman shifts are insufficient to fully truncate the strong form of the intramolecular dipolar couplings; hence, the eigenstates of the system are near, but not equal to, the usual computational basis states.

TABLE I: Zeeman shifts and intramolecular dipolar couplings of the ^{13}C Hamiltonian, columns 1-3 from left; dipolar couplings involving the methylene protons, columns 4-5; ^{13}C free-induction dephasing times (T_2^*) and spin-lattice relaxation times (T_1). Values in columns 1-5 are in kHz.

	C_1	C_2	C_m	H_{m1}	H_{m2}	T_2^* (ms)	T_1 (s)
C_1	5.893	0.227	0.935	-1.5	2.0	2.4	160
C_2		1.057	1.070	1.4	1.0	2.0	325
C_m			-3.445	-18.7	-0.9	1.5	315

B. Experimental setup

All experiments were carried out at room temperature on a Bruker Avance NMR spectrometer operating at a field of 7.1 T, and home-built dual RF channel probe. The sample coil had an inner diameter of 3 mm, and the typical $\pi/2$ 'hard' pulse lengths were $1.25\mu\text{s}$ and $0.75\mu\text{s}$ for carbon and hydrogen, respectively.

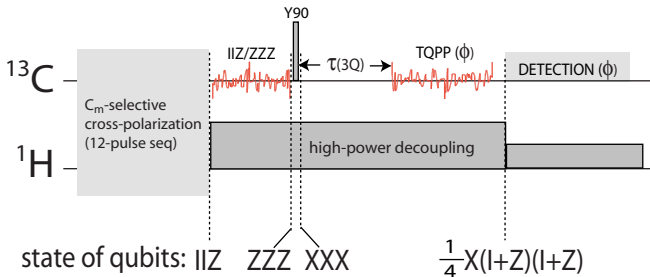


FIG. 4: Schematic pulse sequence for pseudopure state preparation using strongly-modulating pulses. The states of the qubits are indicated in product operator format after each transformation. The state $1^1\mathbb{I}^2Z^m$ is denoted as 'IIZ', for example. Strongly-modulating pulses are represented by waveforms labelled 'IIZ/ZZZ' and 'TQPP', whose durations are 0.54 ms and 1.10 ms, respectively. A collective $\pi/2$ rotation about the rotating-frame Y -axis is labelled 'Y90'. The angle ϕ represents a six-fold phase-shifting of the RF to filter out all coherences except the 3Q coherence. $\tau(3Q)$ indicates a variable delay subsequent to the creation of the 3Q state that is used to measure that state's decay.

IV. PSEUDOPURE STATE

A. Preparation method

A labelled pseudopure state [2, 9] can be prepared in this system using a combination of tailored RF pulses and RF phase cycling (temporal averaging). A schematic of the pulse sequence is shown in Figure 4. The first step is a selective transfer of ^1H polarization to the methylene carbon C_m , utilizing the $^1\text{H}/^{13}\text{C}$ coupling Hamiltonian \mathcal{H}_{CH} . While it is not necessary for this protocol to begin with a *selective* transfer, we demonstrate it here because it may be used in other algorithms for controlled, selective coupling of the qubit system to the bulk ^1H system (which can be considered as a thermal-bath of spin polarization). To accomplish the transfer, an evolution-suspension pulse sequence is applied on both ^1H and ^{13}C channels synchronously, which, by definition, effectively removes $\mathcal{H}_C + \mathcal{H}_H$ from the ensemble Hamiltonian [22, 23]. In such sequences, homonuclear dipolar terms are refocussed by toggling the interaction-frame Hamiltonian along the rotating-frame \hat{x} , \hat{y} and \hat{z} directions, spending equal time along each axis. Therefore, the dual sequence creates (to lowest order in the Magnus expansion of the average Hamiltonian [23]) an effective $^1\text{H}-^{13}\text{C}$ exchange Hamiltonian

$$\mathcal{H}_{\text{eff}} = \sum_{j \in C, k \in H} \frac{D_{jk}}{3} \frac{(Z^j Z^k + Y^j Y^k + X^j X^k)}{2}, \quad (6)$$

where D_{jk} are pairwise $^1\text{H}-^{13}\text{C}$ dipolar coupling constants, and the indices j, k run over all $^{13}\text{C}, ^1\text{H}$ spins, respectively. In the special case that there is only one coupled carbon/proton pair with a coupling of D_{CH} , applica-

tion of the sequence for a time $\tau = 3/(4D_{CH})$ will result in a state exchange between the two nuclei. Since this is approximately the case for the strong methylene $^1\text{H}-^{13}\text{C}$ coupling in our oriented malonic acid system (see Table I), we may implement a *selective* polarization transfer to C_m of magnitude $P \simeq P_H = 3.98P_C$ (P_C and P_H are the thermal equilibrium carbon and proton polarizations, respectively). Furthermore, this selective transfer removes a very small amount of polarization from the ^1H bath, since only the methylene protons on a dilute fraction of ^{13}C -labelled molecules lose their polarization, and the remaining bulk ^1H polarization is preserved under the evolution-suspension sequence. In our system, a selective polarization transfer of about 83% of P_H to C_m was achieved with a 12-pulse subsequence [26] of the Cory 48-pulse sequence [22]; the duration of the 12-pulse sequence was 40 μs for maximum transfer. The thermal equilibrium ^{13}C polarization can be removed prior to such a transfer by rotating the equilibrium ^{13}C state ($\propto Z$) into the transverse ($\hat{x} - \hat{y}$) plane and allowing it to dephase under local ^1H dipolar fields.

Product operator terms denoting qubit states are ordered as $C_1 \otimes C_2 \otimes C_m$; for example, the symbol $\mathbb{1}XZ$ corresponds to the state $\mathbb{1}^1 \otimes X^2 \otimes Z^m$. Also, single-spin terms such as $X^1 \otimes \mathbb{1}^2 \otimes \mathbb{1}^3$ are sometimes abbreviated as X^1 , for example. The polarization transfer is followed by a ^{13}C modulated RF pulse that transforms the state $\mathbb{1}\mathbb{1}Z$ to ZZZ , and then a collective $\pi/2$ pulse that rotates this to XXX . In addition to single-quantum terms, this state contains the triple-quantum (3Q) coherence $\sigma_+ \sigma_+ \sigma_+ + \sigma_- \sigma_- \sigma_-$, where $\sigma_+ = X + iY$ and $\sigma_- = X - iY$. A subsequent modulated pulse (denoted 'TQPP' for 'triple-quantum to pseudopure') transforms the 3Q coherence into the labelled pseudopure state $X(\mathbb{1} + Z)(\mathbb{1} + Z)$. This state is observable as a single NMR transition of C_1 [27]. In order to cancel all other signals arising from the single-quantum terms in the state XXX , phase cycling is used which exploits the n -proportional phase acquisition of an n -quantum state under z -axis rotation. Choosing desired coherence pathways using phase cycling is widely practiced in modern NMR spectroscopy [10]. By shifting the phase of the RF by ϕ during the TQPP pulse, the unitary transformation generated by the pulse is rotated by ϕ about $Z' = Z^1 + Z^2 + Z^m$:

$$U_{tqpp}(\phi) = R_z^\phi U_{tqpp} R_z^{-\phi} \quad (7)$$

where $R_z^\phi \equiv e^{-i(Z')\phi/2}$. Note this is only true since the internal Hamiltonian of the system commutes with Z' , hence a z -axis rotation can be accomplished by acting only on the phase of the RF pulse. We may decompose the state prior to the TQPP pulse into 3Q and single-quantum (1Q) terms, e.g. $XXX = \rho_{\pm 3Q} + \rho_{\pm 1Q}$. The

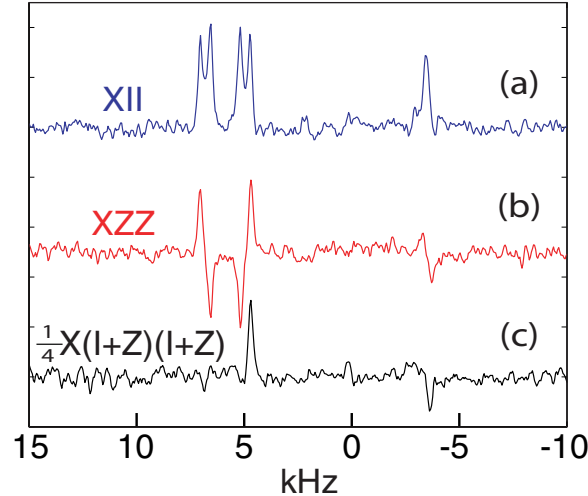


FIG. 5: Experimental results for the pseudopure state protocol. (a) readout of the state $\mathbb{1}\mathbb{1}Z$ just after the selective polarization transfer, with readout consisting of a swap from C_m to C_1 and collective $\pi/2$ pulse about the \hat{y} -axis to produce $X\mathbb{1}\mathbb{1}$; (b) readout of the state ZZZ by a C_1 -selective $\pi/2$ rotation to produce the observable state XZZ ; (c) the labelled pseudopure state yields a single absorption peak from the C_1 multiplet. Fitting the data by spectral simulation indicates a protocol fidelity of 87%, using spectrum (a) as a reference.

final density matrix is calculated as:

$$\begin{aligned} \rho_f(\phi) &= R_z^\phi U_{tqpp} R_z^{-\phi} (\rho_{\pm 3Q} + \rho_{\pm 1Q}) R_z^\phi U_{tqpp}^\dagger R_z^{-\phi} \\ &= R_z^\phi ((e^{-3i\phi} \sigma_+ + e^{3i\phi} \sigma_-) (\mathbb{1} + Z) (\mathbb{1} + Z)/8 + e^{\mp i\phi} \rho') R_z^{-\phi} \end{aligned} \quad (8)$$

where $\rho' = U_{tqpp}(\rho_{\pm 1Q})U_{tqpp}^\dagger$. Incrementing ϕ in units of $\frac{\pi}{3}$ for 6 scans, alternately adding and subtracting, adds constructively the 3Q terms while cancelling the 1Q terms, since

$$\sum_{k=1}^6 (-1)^{k-1} e^{\pm n i k \frac{\pi}{3}} = 6 \cdot \delta(n - 3m), \quad (9)$$

where m is an odd integer, and here $m = 1$ since $n \leq 3$. The remaining z -rotation R_z^ϕ is undone by incrementing the phase of the receiver along with that of the TQPP modulated RF pulse. The labelled pseudopure state is thus obtained:

$$\frac{1}{6} \sum_{k=1}^6 (-1)^{k-1} R_z^{-k\pi/3} \rho_f(k\pi/3) R_z^{k\pi/3} = X(\mathbb{1} + Z)(\mathbb{1} + Z)/4 \quad (10)$$

The amount of signal contained in the resulting pseudopure state is $1/4$ that of the input state, equal to the proportion of 3Q part of the state XXX .

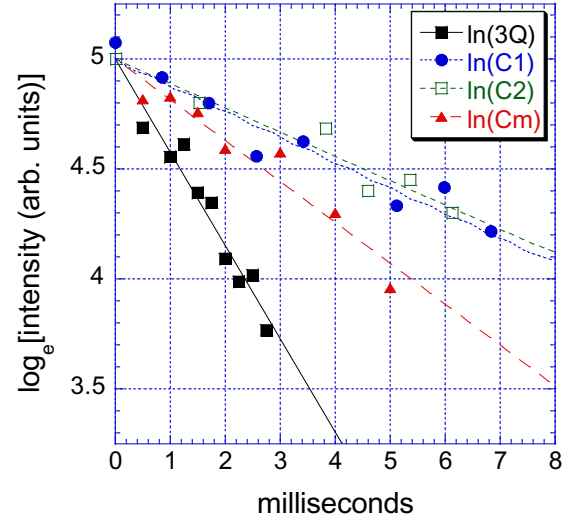


FIG. 6: Triple-quantum (3Q) and single-quantum dephasing data, plotted as the natural log of the signal intensity. Exponential fits indicate decay time constants (in milliseconds) of [2.37 (3Q), 5.37 (C_m), 9.07 (C_2), 8.66 (C_1)].

B. Pseudopure state results

Results for the pseudopure state protocol of Fig. 4 are shown in Fig. 5. It shows (a) readout of the state $\mathbb{1}\mathbb{1}Z$ just after the selective polarization transfer, with readout consisting of a state-swap from C_m to C_1 followed by a collective $\pi/2$ pulse to produce $X\mathbb{1}\mathbb{1}$; (b) readout of the state ZZZ by a C_1 -selective $\pi/2$ rotation to produce the observable state XZZ ; (c) the labelled pseudopure state yields a single absorption peak from the C_1 multiplet. Using the spectrum (a) as reference, the state-correlation fidelity of the pseudopure state protocol, determined by spectral fitting, is 87%. Similarly, the fidelity of the TQPP pulse, using the XZZ spectrum (b) as a reference, is 97%. These results serve as a benchmark for quantum control in the dilute molecular crystal system. They suggest that dephasing due to Zeeman shift dispersion is largely suppressed by these pulses, since the average free-induction dephasing time of the qubits is $T_2^* \simeq 2$ ms, and the total duration of the two modulated pulses, $\simeq 1.6$ ms, is a large fraction of that time.

C. Dipolar dephasing of triple-quantum coherence

Dephasing of the 3Q coherence state $\sigma_+ \sigma_+ \sigma_+ + \sigma_- \sigma_- \sigma_-$ was measured by inserting a variable time delay $\tau(3Q)$ following the 'Y90' pulse in Fig. 4. A collective π pulse was also inserted in the center of $\tau(3Q)$ to refocus Zeeman Hamiltonian terms (Hahn echo), so that the measured dephasing rate reflects

only the perturbing dipolar fields experienced by the nuclei. This 3Q state is significant from a quantum computing perspective since it consists of the two most fragile density matrix elements in the three-qubit system, the extreme off-diagonal elements that are contained in the so-called "cat-state" $|000\rangle + |111\rangle$. The resulting signal decay is shown in Fig. 6 along with the 1Q dephasing data for each qubit, also measured via Hahn echo. The 1Q decay data were measured by first preparing the state X^1 , X^2 or X^m , and using the pair of outer spectral peaks from each spin multiplet to gauge the signal, observing only at delays corresponding to multiples of the dipolar oscillation periods of these peaks. Exponential fits yield decay time constants (in milliseconds) [2.37 (3Q), 5.37 (C_m), 9.07 (C_2), 8.66 (C_1)], with experimental uncertainty $\simeq \pm 11\%$ for each value. Summing the three 1Q dephasing rates predicts a 3Q rate corresponding to a 2.43 ± 0.4 ms time constant, in excellent agreement with the experimental result.

Detailed study of multiple-quantum dephasing rates begs the question of whether or not the dephasing environments of different qubits are correlated or not. For dephasing (or 'noise') environments with Gaussian frequency distributions, correlated decay rates of multiple-quantum coherent states are faster than uncorrelated rates, thereby allowing the degree of noise correlation to be measured [28]. However, Lorentzian noise distributions do not yield any contrast between the correlated and uncorrelated cases [29], so that multiple-quantum dephasing rates are always obtained by summing the appropriate 1Q rates. It will also be shown in the next section that the intermolecular dipolar environment in the dilute malonic acid system has a frequency distribution that is approximately Lorentzian. Hence, multiple-quantum decay rates are not expected to yield any information about qubit noise correlation in this system. On the other hand, the fact that multiple-quantum states in Lorentzian environments will decay at the same rate, whether correlated or not, is advantageous for quantum information processing in such systems.

Finally, we remark that the faster 1Q dephasing of the methylene carbon C_m evident in Fig. 6 is probably due to a residual interaction with its neighboring proton, as the ~ 20 kHz coupling is difficult to completely remove, despite large amplitude decoupling fields. This effect is also evident in the data presented in section V B.

V. CHARACTERIZATION II: INTERMOLECULAR DIPOLAR FIELDS

A. Modelling intermolecular dipolar dephasing

^{13}C - ^{13}C intermolecular dipolar dephasing rates in the dilute crystal architecture can be estimated theoretically for a given labelled-molecule dilution and crystal orienta-

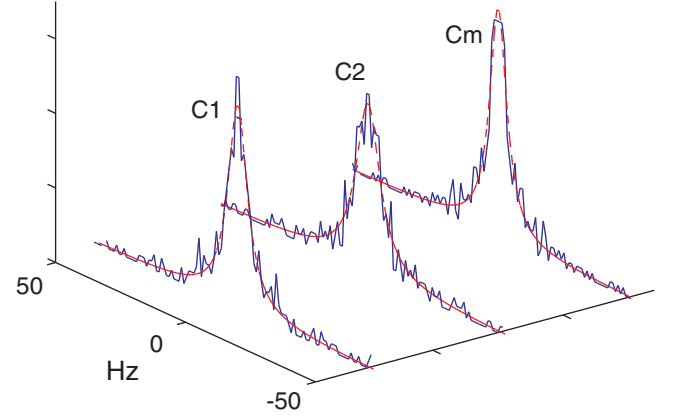


FIG. 7: Simulation of line-shapes resulting from intermolecular dipolar couplings in 1.9% molecular dilution ^{13}C malonic acid. The simulated data (solid lines) are shown with Lorentzian fits (dashed lines). The resulting linewidths (FWHM) for C_1 , C_2 and C_m are 9, 11 and 9 Hz respectively. Correcting for spin diffusion dynamics and the presence of natural abundance spins, the linewidths should be approximately a factor ~ 3.2 broader.

tion, based on the known crystallographic data. We will first outline an approximate, statistical calculation of the static dipolar field spectrum, and then use this result to estimate the further broadening due to spin diffusion dynamics.

Using the Cartesian atomic coordinates obtained by x-ray diffraction [20], as well as the unit cell vectors (\vec{A} , \vec{B} , \vec{C}) (see Fig. 2), vectors were constructed linking each carbon on a reference molecule to each carbon on its unit cell partner and on each of the 52 molecules within the 26 (corner, face or edge) adjacent unit cells (a total of 53 lattice sites). These vectors were then used to calculate all 477 dipolar coupling constants of the form:

$$d_{jk}(r_{jk}, \theta_{jk}) = \gamma_C^2 \hbar \frac{1 - 3\cos^2(\theta_{jk})}{2r_{jk}^3} \quad (11)$$

where γ_C is the gyromagnetic ratio of ^{13}C , r_{jk} is the length of the internuclear vector connecting spins j and k and θ_{jk} is the angle between this vector and the dc magnetic field direction. The set of coupling constants were used to calculate NMR absorption frequencies of a reference spin in the case of single labelled molecule occupancy of one of the 53 lattice sites, at the crystal orientation used in the experiments. This occupancy rate corresponds to a labelled-molecule concentration of $\frac{1}{53} = 1.9\%$. Like-spin C_α - C_α couplings were assigned frequencies $\pm \frac{3}{2}d_{jk}$ (strong-form dipolar coupling), and unlike C_α - C_β couplings were assigned frequencies $\pm d_{jk}$ (dipolar coupling truncated by Zeeman shift). Frequency histograms were obtained by averaging over all 53 lattice sites. Figure 7 shows the resulting histograms for C_1 ,

C_2 and C_m in the crystal orientation used throughout. Lorentzian functions provide excellent fits to the simulated spectra, as expected for a dilute spin system [11]. These correspond to the expected indirect-dimension line-shapes that would result in a two-dimensional NMR experiment under a Hahn echo sequence [10]. The fits yield full-width half-maximum (FWHM) linewidths $\Delta\nu \sim 10$ Hz. The presence of single ^{13}C spins due to natural abundance (1.1% atomic concentration) adds to the total spin concentration. This broadens the linewidth estimate by a factor $\simeq \frac{\eta+1.1\%}{1.9\%}$ for a dilute labelled-molecule percentage $\eta < 10\%$, since linewidth is approximately linear in spin concentration in this dilute regime [11]. Actual dipolar linewidths are expected to be even broader due to spin-diffusion dynamics among like spins. These dynamics cause local field fluctuations $\sim \pm \frac{1}{2}\Delta\nu$; hence, each narrow 'spin packet' in frequency will be broadened over a range $\sim \Delta\nu$, leading to an approximate doubling of the overall linewidth to $\sim 2\Delta\nu$. Taken together, these considerations suggest realistic estimates for the experimental linewidth of $\Delta\lambda \sim 2\frac{\eta+1.1\%}{1.9\%}\Delta\nu$.

These results are summarized in Table II along with experimental data obtained in a 1.6% labelled-molecule dilution crystal. The experimental values indicate effective Lorentzian linewidths of the natural abundance ^{13}C spins measured via Hahn echo, and by a multiple-pulse sequence consisting of the MREV-8 dipolar refocusing sequence [23] in combination with the Hahn echo (detailed in the following section). For comparison with the data obtained in the 1.6% crystal, the simulated linewidths were scaled by a factor 0.9 to yield the correct total spin concentration. In the table, 'Simulation II' refers to the aforementioned linewidth simulations, and the values in parentheses are corrected for spin-diffusion and natural abundance spin concentration. These values should correspond closely to the Hahn echo experimental data, and in fact the agreement with the corrected simulation values is excellent. 'Simulation I' refers to simulations in which like-spin C_α - C_α couplings were omitted, and no spin-diffusion correction made. These values should correspond closely to the dipolar+Hahn refocusing data, since like-spin dipolar couplings, and therefore spin-diffusion, are removed by the sequence.

B. Coherence times under dipolar+Hahn refocusing

Application of a Zeeman and homonuclear dipolar refocusing sequence was investigated, to compare with the simulations of the previous section, and to explore the attainability of long ^{13}C coherence times. The employed sequence is the MREV-8 [23] dipolar decoupling sequence in combination with a Hahn echo. The pulse spacing of the MREV-8 sequence was set such that one eight-pulse cycle was $240\mu\text{s}$ in duration. A single π -pulse was applied

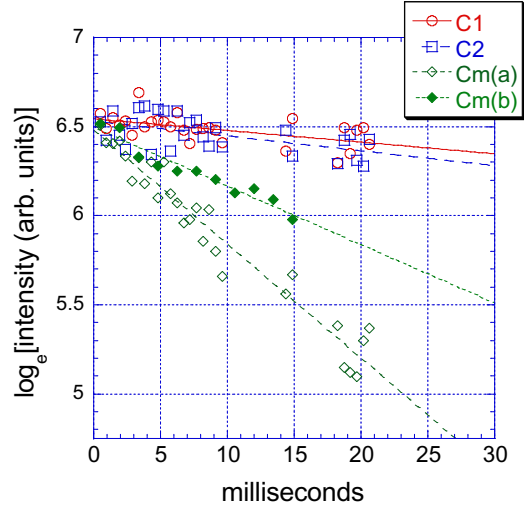


FIG. 8: Decay of signal intensity under the dipolar+Hahn refocusing sequence for natural abundance spins in the 1.6% isotopic dilution crystal. $C_m(a)$ and $C_m(b)$ had TPPM proton decoupling RF power levels of 270 kHz and 330 kHz, respectively. Exponential fits to the data indicate effective coherence times (in milliseconds) of [150 (C_1), 120 (C_2), 16 ($C_m(a)$), 30 ($C_m(b)$)], although clearly the values obtained for the slower C_1 and C_2 decays are more approximate than those for C_m . Dephasing times > 21 ms were not explored here due to the heating effects of high-power proton decoupling on the room temperature probe/sample.

in the center of a given dephasing period for the Hahn echo refocusing of Zeeman terms. It is a quasi-evolution-suspension sequence because it refocusses like-spin dipolar evolution on a relatively short time-scale compared to the refocusing of Zeeman evolution. Therefore it does not fully remove weak-form dipolar couplings such as the unlike-spin C_α - C_β couplings. The data are shown in Figure 8. The decay of the magnetization of the natural abundance spins is shown, since the aim here is to see the effect of refocusing the *intermolecular* dipolar couplings on coherence times. Monitoring the natural abundance spins is ideal in this regard, since the average *intermolecular* dipolar environment is identical for all ^{13}C spins in the sample, and for the natural abundance spins, it is the *only* ^{13}C dipolar environment. On the other hand, efficient refocusing of the *intramolecular* couplings would require a shorter MREV-8 sequence, and therefore more pulses for a given dephasing time, yielding greater loss of signal due to pulse imperfections. The ability to suspend the evolution of the qubit spins (e.g. to generate an effective propagator equal to the identity) is an important benchmark for control [24] and should be explored in future work.

The coherence times of C_1 and C_2 indicated in Fig. 8 (and the corresponding Lorentzian linewidths shown in Table II) demonstrate a ~ 50 -fold increase in coherence

TABLE II: Simulated and experimental dephasing rates for natural abundance spins in 1.6% isotopic dilution crystal, in terms of Lorentzian linewidths (all in Hz). Simulations I/II refer to the exclusion/inclusion of couplings between indistinguishable spins. 'Simulation II' values should be compared to the Hahn echo results, and 'Simulation I' values should be compared to the dipolar+Hahn refocusing results. Under the latter sequence, effective linewidths are reduced by nearly two orders of magnitude compared to the free-induction decay spectrum, with the exception of C_m , whose coherence time is limited by residual proton dephasing (see footnote *a*).

	Dipolar and static-field dephasing (1.6% crystal)				
	Simulation I	dipolar + Hahn refocusing	Simulation II	Hahn echo	FID
C1	2.7	~ 2	8 (26 ^b)	25	133
C2	3.6	~ 3	10 (32 ^b)	32	122
C3	2.7	11/20 ^a	8 (26 ^b)	25	103

^a11 Hz and 20 Hz correspond to proton decoupling powers of 330 kHz and 270 kHz, respectively.

^bValues in parentheses indicate estimated values after making a rough correction for the presence of natural abundance spins and for spin-diffusion dynamics.

time compared with the free-induction dephasing times (Table I), in good agreement with the expected dephasing rate from residual C_α - C_β dipolar interactions. The coherence time of the methylene carbon C_m is clearly limited by the efficiency of proton decoupling. We note that dephasing times > 21 ms were not explored due to the heating effects of high-power proton decoupling on the room temperature probe/sample. Comparing the Hahn echo and dipolar/Hahn echo data, it is seen that Zeeman shift dispersion contributes ~ 90 Hz to the free-induction linewidths, whereas the intermolecular dipolar fields contribute ~ 25 Hz. Sequences that efficiently average all spin interactions, including unlike-spin couplings, could be used to test the limits of line-narrowing. One such sequence is the Cory 48-pulse sequence [22].

VI. DISCUSSION

In this paper, we have established benchmark results and described a methodology for controlling solid-state NMR qubits upon which future work can build and improve. High-fidelity quantum control was demonstrated through the preparation of a pseudopure state. That result, along with unitary fidelity simulations for the 3-qubit controlled-(not \otimes not) gate, suggests that ensemble inhomogeneities involving linear Hamiltonian terms (Zeeman dispersion, RF amplitude) may be suppressed by strongly modulating RF pulses. Additionally, the method of strongly-modulating pulses is well-suited to finding near time-optimal solutions to complex quantum gates. Measurement of the triple-quantum dipolar dephasing rate was carried out, as an application of the pseudopure state protocol. Simulations of the intermolecular dipolar field spectrum predicted dipolar linewidths in excellent agreement with experimental results obtained under appropriate refocusing sequences. Refocusing of the dominant Zeeman and dipolar terms lead to a 50-fold increase in ensemble coherence times,

and suggests that much narrower effective linewidths could be achieved using sequences that efficiently remove all spin interactions.

These results demonstrate the potential for achieving universal quantum control in solid-state NMR systems with the high precision required for quantum computation and information processing. Coupled with state purification techniques like dynamic nuclear polarization, such control should enable a powerful new testbed for quantum computing reaching up to $\sim 20 - 30$ qubits [5]. Furthermore, the solid-state setting is much more general than the liquid-state, for example, allowing to couple the qubits to a bulk-spin heat bath [5], as demonstrated by the selective polarization transfer that was employed to begin the pseudopure state protocol. Similar techniques will enable implementation of quantum error correction and heat-bath algorithmic cooling [13] protocols, the latter of which was already demonstrated in the malonic acid system [14].

To further improve control, the strongly modulating pulse optimization procedure must be improved to yield simulated fidelities comparable to those achievable in the liquid state (that is, unitary fidelities in the range of 99 – 99.9% as opposed to $\sim 95 - 99\%$). Moreover, the experimental system must be carefully engineered so that the implemented control fields are sufficiently faithful to the simulated pulses. Extending to larger numbers of qubits ($\gtrsim 12$) will likely require some form of hybrid control that utilizes multiple-pulse, average Hamiltonian techniques in combination with the numerical optimization methods discussed. Additionally, scalable control methods that have been successfully demonstrated in the weak-coupling regime [6, 8] could potentially be merged with the strongly modulating pulse methodology to achieve a scalable pulsefinder for general systems.

In conclusion, we have characterized in detail a novel solid-state NMR system for quantum information processing, and used it to demonstrate high-fidelity quantum control. These lay the foundation for future studies

in the malonic acid system, and in larger systems, desirably with high polarization.

Acknowledgments

We wish to acknowledge NSERC, CIAR, ARDA, ARO and LPS for support; M. Ditty, N. Taylor and W. Power

for experimental assistance.

[1] M. A. Nielsen and I. L. Chuang, *Quantum Computation and Quantum Information* (Cambridge University Press, Cambridge, UK, 2000).

[2] D. G. Cory, M. D. Price, and T. F. Havel, *Physica D* **120**, 82 (1998), quant-ph/9709001.

[3] I. L. Chuang, N. Gershenfeld, M. Kubinec, and D. Leung, **454**, 447 (1998).

[4] C. S. Yannoni, M. H. Sherwood, L. M. K. Vandersypen, D. C. Miller, M. G. Kubinec, and I. Chuang, *Appl. Phys. Lett.* **75**, 3563 (1999), quant-ph/9908012.

[5] D. G. Cory, R. Laflamme, E. Knill, L. Viola, T. F. Havel, N. Boulant, G. Boutis, E. Fortunato, S. Lloyd, R. Martinez, et al., *Fort. der Phys. special issue, Experimental Proposals for Quantum Computation* **48** (2000), quant-ph/0004104.

[6] E. Knill, R. Laflamme, R. Martinez, and C.-H. Tseng, *Nature* **404**, 368 (2000), quant-ph/9908051, URL <http://www.ariv.org/abs/quant-ph/9908051>.

[7] R. Das, R. Bhattacharyya, and A. Kumar, *J. Magn. Res.* **170**, 310 (2004).

[8] C. Negrevergne, T. S. Mahesh, C. A. Ryan, N. Boulant, M. Ditty, F. Cyr-Racine, W. Power, T. F. Havel, D. G. Cory, and R. Laflamme, in submission (2005).

[9] E. Knill, I. Chuang, and R. Laflamme, *Phys. Rev. A* **57**, 3348 (1998), quant-ph/9706053.

[10] R. R. Ernst and G. Bodenhausen, *Principles of Nuclear Magnetic Resonance in One and Two Dimensions* (Clarendon Press, Oxford, UK, 1987).

[11] A. Abragam, *Principles of Nuclear Magnetism* (Clarendon Press, Oxford, England, 1961).

[12] A. Abragam and M. Goldman, *Nuclear Magnetism: Order and Disorder* (Oxford University Press, Oxford, England, 1982).

[13] L. Schulman and U. Vazirani, Proc. of the 31th Annual ACM Symposium on Theory of Computing p. 322 (1990).

[14] J. Baugh, O. Moussa, C. A. Ryan, A. Nayak, and R. Laflamme, *Nature accepted* **9-2005** (2005).

[15] E. Knill, R. Laflamme, and W. H. Zurek, *Science* **279**, 342 (1998).

[16] R. Laflamme, C. Miquel, J.-P. Paz, and W. H. Zurek, *Phys. Rev. Lett.* **77**, 198 (1996).

[17] G. M. Leskowitz, R. A. Olsen, N. Ghaderi, and L. J. Mueller, *J. Chem. Phys.* **119**, 1643 (2003).

[18] E. M. Fortunato, M. A. Pravia, N. Boulant, G. Tekle-mariam, T. F. Havel, and D. G. Cory, *J. Chem. Phys.* **116**, 7599 (2002).

[19] J.-S. Lee and A. K. Khitrin, *Phys. Rev. A* **70**, 022330 (2004).

[20] N. R. Jagannathan, S. S. Rajan, and E. Subramanian, *J. Chem. Cryst.* **24**, 75 (1994).

[21] A. E. Bennett, C. M. Rienstra, M. Auger, K. V. Lakshmi, and R. G. Griffin, *J. Chem. Phys.* **103**, 6951 (1995).

[22] D. G. Cory, J. B. Miller, and A. N. Garroway, *J. Mag. Res.* **90**, 205 (1990).

[23] U. Haeberlen, *High Resolution NMR in Solids: Selective Averaging* (Academic Press, New York, USA, 1976).

[24] T. D. Ladd, D. Maryenko, Y. Yamamoto, E. Abe, and K. M. Itoh, *Phys. Rev. B* **71**, 014401 (2005).

[25] Crystal strain would, in general, also lead to a dispersion of qubit-qubit dipolar couplings.

[26] The 12-pulse subsequence does not fully average to zero all interactions even to 0^{th} -order, so it is not strictly an evolution-suspension sequence. On the other hand, the duration of the transfer is short enough that the evolution operator of the bulk spin system is very close to the identity operator.

[27] This is only approximately true; a small amount of the pseudopure signal will be found on other spin transitions due to the strong coupling effect. In this experiment, such weak signals are not separable from the noise, although the effect is taken into account when spectrally fitting the data.

[28] D. Simon, J. C. Boileau and R. Laflamme, unpublished

[29] This can be verified, e.g. in a two-qubit system, by taking the cases of identical versus uncorrelated qubit environments. Appropriate evaluation of the 2-quantum dephasing rate in both cases yields the same rate for a Lorentzian-distributed environment, in contrast to a Gaussian-distributed one, which yields a factor of two difference between the two rates.